Research Article | Vol. 24, No. 17 | 22 Aug 2016 | OPTICS EXPRESS 19517

Optics EXPRESS

Grating-coupled Otto configuration for hybridized surface phonon polariton excitation for local refractive index sensitivity enhancement

SUEJIT PECHPRASARN,[1,2] SUPANNEE LEARKTHANAKHACHON,[1] GAIGE ZHENG,[3] HONG SHEN,[1] DANG YUAN LEI,[4,*] AND MICHAEL G. SOMEKH[1,*]

[1]*Department of Electronic and Information Engineering, Hong Kong Polytechnic University, Hong Kong SAR, China*
[2]*Biomedical Engineering Program, Department of Physics, Faculty of Science, Rangsit University, Pathum Thani, Thailand*
[3]*School of Physics and Optoelectronic Engineering, Nanjing University of Information Science & Technology, Nanjing 210044, China*
[4]*Department of Applied Physics, The Hong Kong Polytechnic University, Hong Kong SAR, China*
[*]*dylei@polyu.edu.hk, mike.somekh@polyu.edu.hk*

Abstract: We demonstrate numerically through rigorous coupled wave analysis (RCWA) that replacing the prism in the Otto configuration with gratings enables us to excite and control different modes and field patterns of surface phonon polaritons (SPhPs) through the incident wavelength and height of the Otto spacing layer. This modified Otto configuration provides us the following multiple modes, namely, SPhP mode, Fabry-Pérot (FP) cavity resonance, dielectric waveguide grating resonance (DWGR) and hybridized between different combinations of the above mentioned modes. We show that this modified grating-coupled Otto configuration has a highly confined field pattern within the structure, making it more sensitive to local refractive index changes on the SiC surface. The hybridized surface phonon polariton modes also provide a stronger field enhancement compared to conventional pure mode excitation.

OCIS codes: (050.2230) Fabry-Perot; (240.6690) Surface waves; (050.6624) Subwavelength structures; (050.1950) Diffraction gratings.

References and links

1. B. G. Ghamsari, X. G. Xu, L. Gilburd, G. C. Walker, and P. Berini, "Mid-infrared surface phonon polaritons in boron-nitride nanotubes," J. Opt. **16**, 114008 (2014).
2. K. Tsushima, S. Mori, Y. Nishimura, K. Hishii, K. Kasahara, T. Yaji, H. Miyazaki, N. Ikeda, M. Ochiai, H. Oosato, and Y. Sugimoto, "Observation of the enhancement of the electric field normal to the surface of mid-infrared slot antennas," in "IEEE 2013 7th International Congress on Advanced Electromagnetic Materials in Microwaves and Optics," (IEEE, 2013), pp. 508–510.
3. X. G. Xu, J.-H. Jiang, L. Gilburd, R. G. Rensing, K. S. Burch, C. Zhi, Y. Bando, D. Golberg, and G. C. Walker, "Mid-infrared polaritonic coupling between boron nitride nanotubes and graphene," ACS Nano **8**, 11305–11312 (2014).
4. S. Basu, Y. Yang, and L. Wang, "Near-field radiative heat transfer between metamaterials coated with silicon carbide thin films," Appl. Phys. Lett. **106**, 033106 (2015).
5. D.-Z. A. Chen and G. Chen, "Heat flow in thin films via surface phonon-polaritons," Front. Heat Mass Transf. **1**, 023005 (2010).
6. M. Francoeur, M. P. Mengüç, and R. Vaillon, "Control of near-field radiative heat transfer via surface phonon–polariton coupling in thin films," Appl. Phys. A **103**, 547–550 (2011).
7. T. Tokunaga, L. Tranchant, N. Takama, S. Volz, and B. Kim, "Experimental study of heat transfer in micro glass tubes mediated by surface phonon polaritons," J. Phys.: Conf. Ser. **395**, 012108 (2012).
8. B. Neuner III, D. Korobkin, C. Fietz, D. Carole, G. Ferro, and G. Shvets, "Critically coupled surface phonon-polariton excitation in silicon carbide," Opt. Lett. **34**, 2667 (2009).
9. N. Dmitruk, T. Barlas, I. Dmitruk, S. Kutovyi, N. Berezovska, J. Sabataityte, and I. Simkiene, "IR reflection, attenuated total reflection, and raman scattering of porous polar III–V semiconductors," Phys. Stat. Solidi (B) **247**, 955–961 (2010).

#268689 http://dx.doi.org/10.1364/OE.24.019517
Journal © 2016 Received 28 Jun 2016; revised 3 Aug 2016; accepted 8 Aug 2016; published 15 Aug 2016

Optics EXPRESS

10. R. H. Hussein, O. Pagès, F. Firszt, W. Paszkowicz, and A. Maillard, "Near-forward raman scattering by bulk and surface phonon-polaritons in the model percolation-type ZnBeSe alloy," Appl. Phys. Lett. **103**, 071912 (2013).
11. A. Otto, "Excitation of nonradiative surface plasma waves in silver by the method of frustrated total reflection," Z. Angew. Phys. **216**, 398–410 (1968).
12. C. Ropers, C. C. Neacsu, T. Elsaesser, M. Albrecht, M. B. Raschke, and C. Lienau, "Grating-coupling of surface plasmons onto metallic tips: a nanoconfined light source," Nano Lett. **7**, 2784–2788 (2007).
13. P. K. Mishra and B. Sahoo, "Growth of amorphous carbon and graphene on pulse laser deposited SiC films and their characterization studies," Laser Part. Beams **31**, 63–71 (2012).
14. T. A. Friedmann, P. B. Mirkarimi, D. L. Medlin, K. F. McCarty, E. J. Klaus, D. R. Boehme, H. A. Johnsen, M. J. Mills, D. K. Ottesen, and J. C. Barbour, "Ion-assisted pulsed laser deposition of cubic boron nitride films," J. Appl. Phys. **76**, 3088 (1994).
15. T. Terasako, H. Song, H. Makino, S. Shirakata, and T. Yamamoto, "Temperature dependence of electrical properties of Ga-doped ZnO films deposited by ion plating with DC arc discharge," Thin Solid Films **528**, 19–25 (2013).
16. O. M. Nayfeh, A. G. Birdwell, C. Tan, M. Dubey, H. Gullapalli, Z. Liu, A. L. M. Reddy, and P. M. Ajayan, "Increased mobility for layer-by-layer transferred chemical vapor deposited graphene/boron-nitride thin films," Appl. Phys. Lett. **102**, 103115 (2013).
17. J. Provine, C. Roper, J. A. Schuller, M. L. Brongersma, R. Maboudian, and R. T. Howe, "The dependence of poly-crystalline SiC mid-infrared optical properties on deposition conditions," in "2008 IEEE/LEOS International Conference on Optical MEMs and Nanophotonics," (IEEE, 2008), pp. 182–183.
18. S. Lee, S. Ng, K. Saw, Z. Hassan, and H. A. Hassan, "Surface phonon polariton characteristics of bulk wurtzite ZnO crystal," Physica B **406**, 115–118 (2011).
19. A. A. Hamilton, T. Dumelow, T. J. Parker, and S. R. P. Smith, "Far infrared attenuated total reflection spectroscopy for investigating superlattice phonon parameters," J. Phys.: Condens. Matter **8**, 8027–8039 (1996).
20. Y. Chen, Y. Francescato, J. D. Caldwell, V. Giannini, T. W. W. Maß, O. J. Glembocki, F. J. Bezares, T. Taubner, R. Kasica, M. Hong, and S. A. Maier, "Spectral tuning of localized surface phonon polariton resonators for low-loss mid-IR applications," ACS Photon. **1**, 718–724 (2014).
21. D. Ju, Y. Jiang, and H. Pei, "Controllable mode hybridization and interaction within a plasmonic cavity formed by two bimetallic gratings," Plasmonics **8**, 1387–1394 (2013).
22. S. S. Wang and R. Magnusson, "Theory and applications of guided-mode resonance filters," Appl. Opt. **32**, 2606 (1993).
23. W. Zhou, Y. Wu, M. Yu, P. Hao, G. Liu, and K. Li, "Extraordinary optical absorption based on guided-mode resonance," Opt. Lett. **38**, 5393 (2013).
24. H. W. Icenogle, B. C. Platt, and W. L. Wolfe, "Refractive indexes and temperature coefficients of germanium and silicon," Appl. Opt. **15**, 2348 (1976).
25. B. Tatian, "Fitting refractive-index data with the sellmeier dispersion formula," Appl. Opt. **23**, 4477 (1984).
26. H. H. Li, "Refractive index of alkali halides and its wavelength and temperature derivatives," J. Phys. Chem. Ref. Data **5**, 329 (1976).
27. V. Karagodsky and C. J. Chang-Hasnain, "Physics of near-wavelength high contrast gratings," Opt. Express **20**, 10888 (2012).
28. L. Wang, B. Lee, X. Wang, and Z. Zhang, "Spatial and temporal coherence of thermal radiation in asymmetric fabry–perot resonance cavities," Int. J. Heat Mass Transf. **52**, 3024–3031 (2009).
29. L. P. Wang, S. Basu, and Z. M. Zhang, "Direct measurement of thermal emission from a fabry–perot cavity resonator," J. Heat Transf. **134**, 072701 (2012).
30. P. Berini, "Long-range surface plasmon polaritons," Adv. Opt. Photon. **1**, 484 (2009).
31. D. Y. Lei, J. T. K. Wan, and H. C. Ong, "Numerical and analytical evaluations of the sensing sensitivity of waveguide mode in one-dimensional metallic gratings," Nanotechnology **23**, 275501 (2012).
32. G. Dolling, H. G. Smith, R. M. Nicklow, P. R. Vijayaraghavan, and M. K. Wilkinson, "Lattice dynamics of lithium fluoride," Phys. Rev. **168**, 970–979 (1968).

1. Introduction

Photon coupled surface phonon polaritons (SPhPs) are guided mechanical surface waves arising from lattice vibrations propagating along the surface of polar crystalline materials, such as, SiC, GaN, wurtzite ZnO and GaAs, which can be optically excited in the mid infrared wavelength ranging from 10 to 15 μm [1–3]. Recently, the SPhPs have been of interest in science and engineering research community since (i) they provide analogous properties to those exhibited by surface plasmon polaritons(SPPs) at a considerably longer wavelength and (ii) they are a potential candidate for sensing mechanical properties, since the optically excited waves manifest themselves as a mechanical vibration. They can thus be used for sensing properties such as,

Optics EXPRESS

pressure and heat conductivity [4–7]. The properties of SPhPs are determined largely by the real part of the permittivity becoming negative, so, like SPPs, they are sensitive to local refractive index and have a substantial field enhancement effect, which makes them attractive for Raman measurement in mid-infrared wavelengths [8–10].

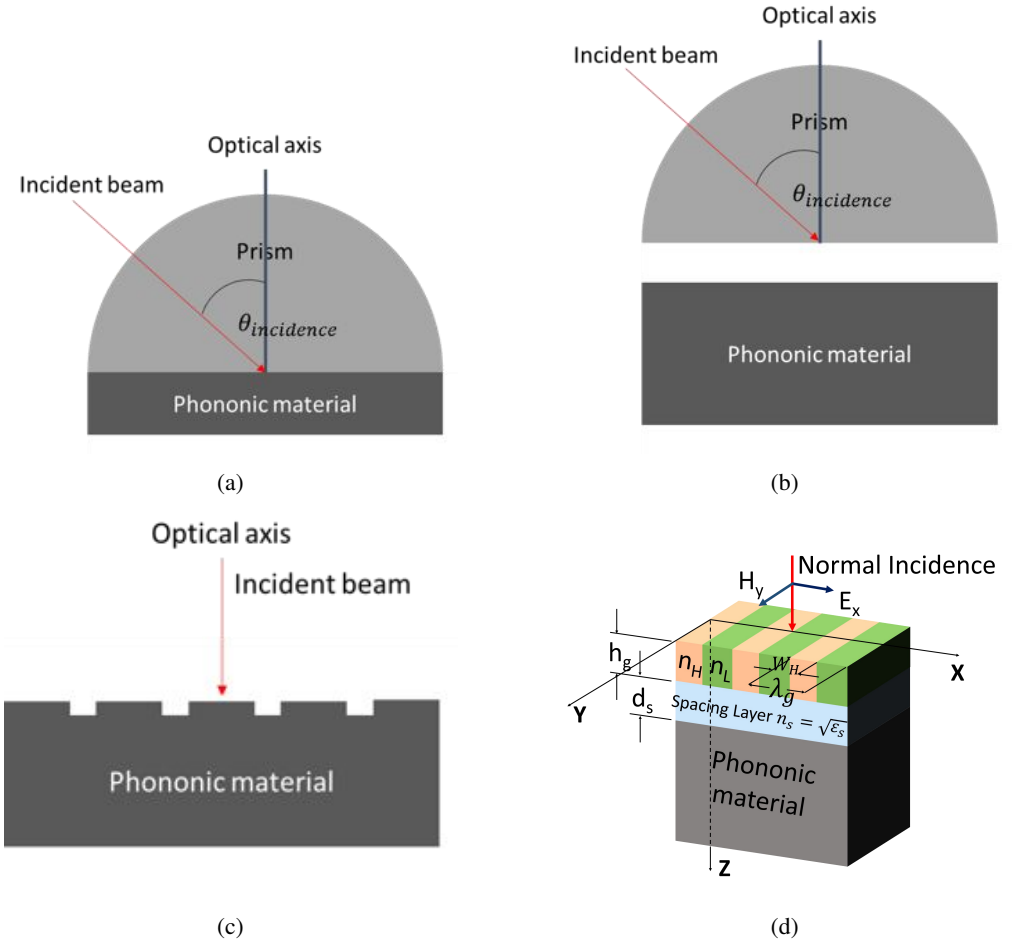

Fig. 1. Four schemes for excitation of SPhPs. (a) prism based Kretschmann configuration, (b) prism based Otto configuration, (c) grating coupled SPhPs, and (d) modified grating-coupled Otto configuration. Different field distributions of this structure are shown in Fig. 8

Similar to SPPs the SPhPs can only be excited with (i) p-polarized light and (ii) evanescent field coupling [8]. In order to ensure evanescent field coupling, the obvious choices are (i) using a high index prism employing either Kretschmann configuration or Otto configuration [11] as shown in Figs. 1(a) and 1(b) respectively or (ii) a grating [12] as shown in Fig. 1(c). The Kretschmann configuration requires thin film deposition on a high index prism. There are a number of research papers investigating the SPhP performance after thin film deposition [13–16], and in general they found that the quality of resonance response was quite poor and the property of the phononic material is dependent on the deposition conditions, such as temperature and pressure [17]. For the Otto configuration, although the method does not require thin film deposition, the results published so far do not show as good a phononic response as expected [18, 19]. Some of the problems associated with the Otto configuration arise from the difficulties in controlling the

Optics EXPRESS

incident angle and the Otto spacing layer gap. The other method to excite SPhPs is to employ a grating in order to increase the k-vector of the incident photons [20];this can be done by electron beam lithography patterning directly onto the phononic material surface. The performance of the e-beam fabricated phononic devices was not consistent and resulted in a much wider SPhP dip. Chen *et al*. [20] attributed this unfavorable performance to the surface damage during plasma etching.

In this paper, we propose a modified grating-coupled Otto configuration, where the prism in Fig. 1(b) is replaced by a dielectric subwavelength grating as shown in Fig. 1(d). This allows one to perform grating-coupled SPhP excitation without a need of e-beam writing or plasma treatment on the surface of phononic material. The grating has advantages over the prism because it provides a wider range of k-vectors to excite phonons due to grating diffracted orders. We also introduce a spacing layer between the grating and the phononic material so that this is essentially an Otto configuration.

In the results section, we demonstrate four key features of the proposed structure which are:

a) Capability to excite different resonant modes and hybridized modes

b) Field enhancement of SPhPs on the surface of phononic material

c) Field confinement on the surface of phononic material and hence improvement in local refractive index sensitivity and figure of merit

d) Controllable operating position of resonances by changing the spacing layer index and thickness

To the authors' knowledge, this simple structure to produce hybridized SPhPs has not been reported before. There is a similar work by Ju *et al*. [21], where they used a sandwiched double layered bimetallic grating structure with dielectric material designed for plasmonic mode hybridization. The hybridization is caused by SPPs excited by evanescent orders of bimetallic grating and Fabry-Pérot (FP) cavity only. The present work uses a simpler structure to demonstrate hybridized modes arising from SPhPs, FP and dielectric waveguide grating resonance (DWGR) and develop a theoretical framework to explain sensitivity enhancement of the structure due to mode hybridizations.

2. Simulation procedure

In this work, we study SiC as the phononic material having the complex permittivity expressed by the Drude-Lorentz model [8] in the absence of free charge carriers. The frequency dependent permittivity of SiC, $\varepsilon_{SiC}(\omega)$, is given by:

$$\varepsilon_{SiC}(\omega) = \varepsilon_{\infty}\frac{\omega^2 - \omega_{LO}^2 + i\gamma\omega}{\omega^2 - \omega_{TO}^2 + i\gamma\omega} \tag{1}$$

where the longitudinal optical phonon frequency, ω_{LO}, = 972 cm^{-1} at λ_{LO} = 10.288 μm, the transverse optical phonon frequency, ω_{TO}, = 796 cm^{-1} at λ_{TO} = 12.563 μm, the damping rate due to vibrational anharmonicity, γ, = 3.75 cm^{-1}, and the high frequency dielectric constant, ε_{∞}, = 6.5. The Reststrahlen band defined where $\Re(\varepsilon_{SiC}) < 0$ corresponds to $\omega_{TO} < \omega < \omega_{LO}$ is shown in Fig. 2.

Results presented in this paper were calculated by Rigorous Coupled Wave Analysis (RCWA) written in MATLAB. All the calculations have been tested for convergence and calculated with the number of diffracted orders equal to 203, which gives the smallest feature size of 8 μm/101 $\approx$ 80 nm.

Optics EXPRESS

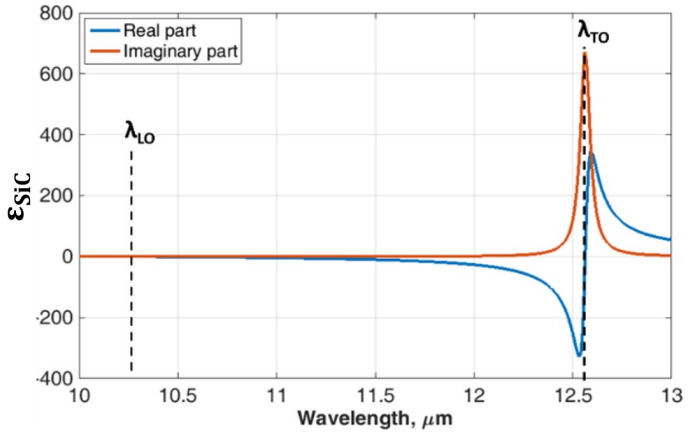

Fig. 2. shows complex permittivity of SiC as calculated by the Drude model with ω_{LO} = 972 cm^{-1} at λ_{LO} = 10.288 μm, the transverse optical phonon frequency ω_{TO} = 796 cm^{-1} at λ_{TO} = 12.563 μm, the damping rate due to vibrational anharmonicity γ = 3.75 cm^{-1}, and the high-frequency dielectric constant ε_∞ = 6.5.

3. Results and discussion

The grating structure shown in Fig. 1(d) was assigned the following parameters to ensure that it generates DWGR [22, 23] n_H=4 (Germanium, Ge [24]), n_L=2.4 (Zinc Selenide, ZnSe [25]), W_H=3.6 μm, λ_g=8.0 μm, h_g=3.8 μm and n_s=1.02 (LiF spacer [26]). Surface-normal reflectance as a function of spacing layer thickness and incident wavelength is shown in Fig. 3(a), where only the zeroth order was propagating and the other modes were evanescent. Multiple reflectance dips and mode hybridizations are observed in Fig. 3(a). The detailed discussions about the resonance modes and their interactions will be given in this subsection along with the comparison with Fig. 3.

3.1. Surface phonons (SPhPs)

SPhPs are generated from different diffracted orders from the grating. We present a heuristic model to estimate the position of the SPhP modes generated by each grating order; this allows us to identify the SPhP branches depicted in Fig. 3. Although the model is approximate with a few underlying approximations it is surprisingly accurate and allows unambiguous identification of the modes. The k-vector of a diffracted order for normal incidence is equal to an integer multiple of the grating vector. Excitation from the mth order diffraction must therefore always have a grating vector given by mk_g, that is

$$k_{xm} = mk_g = m\frac{2\pi}{\lambda_g} \tag{2}$$

where k_{xm} is the k-vector of the mth (evanescent) order and λ_g is the grating period (8 μm in this case). To estimate the wavelength at which the SPhP is excited we take a value of the spacing, d_s and determine an effective permittivity, ε_{eff} seen by the SPhP. We then need to determine whether there is a wavelength at which the phonon wave vector matches the value of k_{xm}. To obtain phonon wave vector we use the usual dispersion relation given by equation 3 below:

$$k_{phonon}(\lambda_0) = \frac{2\pi}{\lambda_0}\sqrt{\frac{\varepsilon_{SiC}(\lambda_0)\varepsilon_{eff}}{\varepsilon_{SiC}(\lambda_0)+\varepsilon_{eff}}} \tag{3}$$

Optics EXPRESS

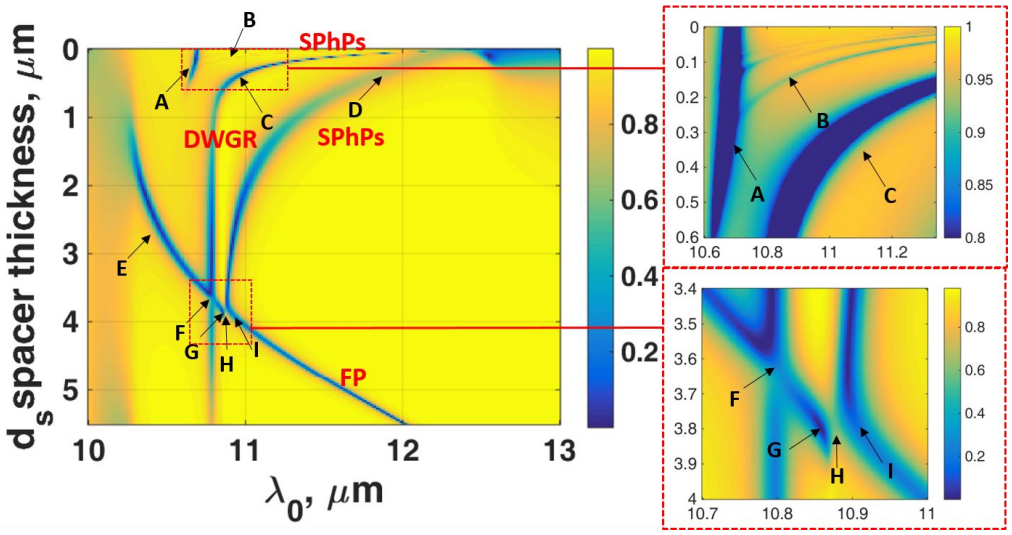

(a)

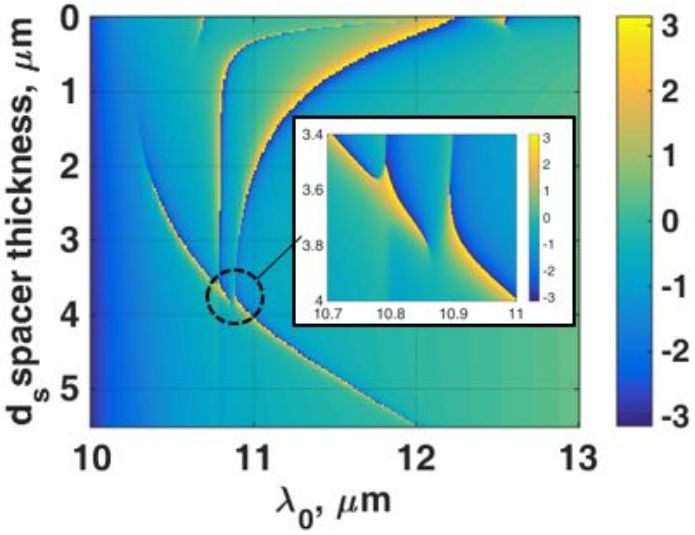

(b)

Fig. 3. shows (a) the simulated zeroth order reflectance for the system shown in Fig. 1(d) as a function of spacer thickness d_s and incident wavelength λ_0 with normal incidence and the electric field parallel to the grating vector and (b) corresponding phase profile (radians) of the zeroth order reflectance.

where k_{phonon} is the phonon k-vector when the incident light is p-polarized, λ_0 is the free space wavelength, ε_{SiC} is the complex permittivity of SiC, and ε_{eff} is the effective permittivity seen by field penetration of the phonon.

In the Otto configuration the surface wave sees the gap as well as the coupling medium (prism or grating, see Fig. 4(a). This is the reason we write the dispersion equation with an effective permittivity, ε_{eff}. In order to determine whether the k-vector of the phonon matches the value we need to estimate ε_{eff}.

Optics EXPRESS

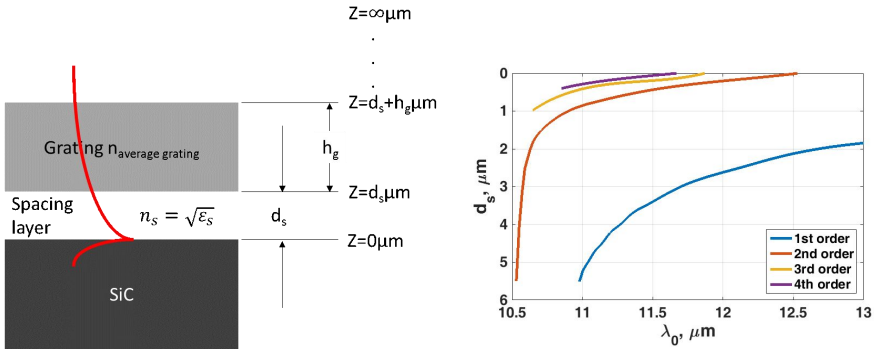

(a) (b)

Fig. 4. (a) shows penetration depth and refractive index seen by phonon field. (b) shows the lines where k_{phonon} match the k_g calculated from the approximate dispersion relation for the 1^{st} diffracted order (blue), 2^{nd} diffracted order (red), 3^{rd} diffracted order (yellow) and 4^{th} diffracted order (magenta) as a function of spacing layer thickness and incident wavelength.

We determine the k-vectors along the z-axis, k_z for each evanescent order by:

$$k_z(\lambda_0) = \sqrt{(\frac{2\pi\sqrt{\varepsilon_s}}{\lambda_0})^2 - k_{xm}^2(\lambda_0)} \tag{4}$$

where ε_s is the spacing layer permittivity. We then use the following weighted average to estimate $\varepsilon_{eff}(d_s)$.

$$\varepsilon_{eff} = n_{eff}^2 = \left| \frac{\int_{z=0}^{z=d_s} n_s e^{-ik_z z} dz + \int_{z=d_s}^{z=d_s+h_g} n_{grating} e^{-ik_z z} dz + \int_{z=d_s+h_g}^{z=\infty} e^{-ik_z z} dz}{\int_{z=0}^{z=\infty} e^{-ik_z z} dz} \right| \tag{5}$$

where n_{eff} is the effective refractive index seen by surface phonons, d_s is the spacer layer thickness, h_g is the grating thickness, n_s is the refractive index of spacing layer, $n_{grating}$ is the average refractive index of grating calculated by $\left[n_H W_H + n_L(\lambda_g - W_H)\right]/\lambda_g$.

This allows us to estimate ε_{eff} as a function of wavelength for a particular separation. The wavelength where the SPhPs are excited must correspond to a situation where the allowable k_{xm} values from the grating (for normal incidence multiples of the grating vector) match the k-vectors from the SPhP dispersion relation. Using this approach, we determine k_{phonon} for each diffracted order as a function of the spacer thickness d_s(and hence ε_{eff}). The presence of these lines indicates the possibility of exciting SPhPs but, of course, says nothing about the strength of excitation. The curves corresponding to each evanescent order are shown in Fig. 4(b) corresponding to m = 1, 2, 3 and 4, respectively.

Figure 4(b) shows that the first diffraction order (blue) does not appear to excite SPhPs, because the SPhP only exists for large gap separations. At these separations, the evanescent wave emerging from the grating is very weak when it arrives at the SiC, so there is little observable SPhP excitation. The phononic responses due to the second (red) and the third (yellow) diffraction orders calculated with the simple dispersion model appear in the positions very close to the dips labeled‘C’ and ‘D’ in Fig. 3(a). In fact, there is a faint arc along the label ‘B’ in Fig. 3(a), and this corresponds to the dispersion relation corresponding to excitation by the 4^{th} diffracted order (magenta). The reason that the coupling strength between the SPhP and the fourth diffraction order is very weak is that the evanescent field magnitude of the 4^{th} order from a rectangular

Optics EXPRESS

grating is very small. We have demonstrated that this simple dispersion model gives an insight into phononic excitation and coupling and predicts which grating orders will be most effective in SPhP excitation. There is, as expected, some deviation between the RCWA calculation and the simplified dispersion model. This is due to the fact that the simple calculation for ε_{eff} does not account for multiple reflections inside the spacing layer, the phonon scattering due to the grating and mode hybridization with other resonances. It is, however, a very useful tool to develop an intuitive understanding.

3.2. Dielectric waveguide grating resonance (DWGR)

In this section we identify the DWGR modes and aid this process by adjusting the parameters of the SiC as discussed in the following paragraph. DWGR are resonances when the grating operates within the guided mode resonance regime as described by the following equation, valid for lossless dielectrics [22].

$$max\{n_{inc}, n_s\} \leq \left|n_{avg\ grating}\right| < n_g \tag{6}$$

where n_{inc} is the refractive index of the incident layer, n_s is the refractive index of the spacing layer, $n_{avg\ grating}$ is the average refractive index value of the grating, n_g is the average refractive index of the grating.

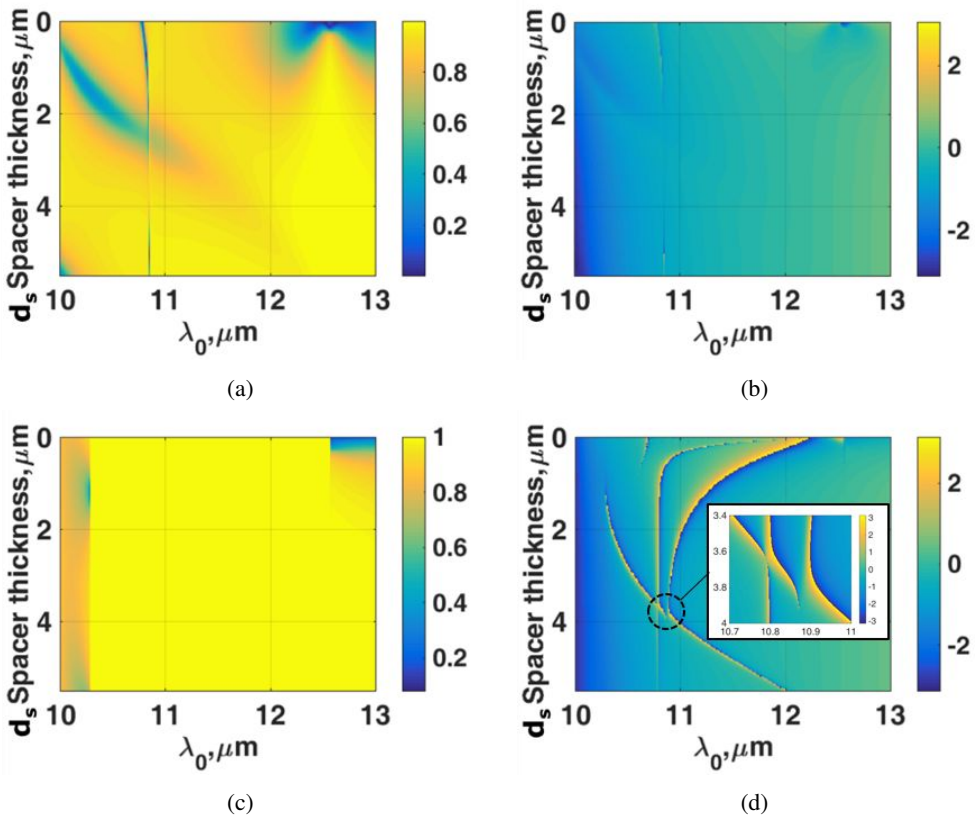

Fig. 5. (a) zeroth order reflectance as a function of spacer thickness d_s and incident wavelength λ_0 with normal incidence and the electric field parallel to the grating vector for case (i) and (b) corresponding phase profile of the zeroth order reflectance for case (i) (real part of complex permittivity is zero, that is no SPhP excitation). (c) and (d) show similar results to (a) and (b) for case (ii) (imaginary part of complex permittivity is zero, no losses).

Optics EXPRESS

In order to identify the different modes we can modify the properties of the SiC substrate in the simulations thus selectively suppressing various modes as follows:

(i) treat real part of complex permittivity of SiC as zero and keep the imaginary part the same, and

(ii) keep the real part of the complex permittivity of SiC the same but treat its imaginary part as zero.

While these will not, of course, represent real material they do provide a nice vehicle to perform a computer experiment for modal identification.

In this work, the grating was engineered to provide evanescent wave excitation and excite SPhPs, nevertheless, it supports strong DWGR modes. There are a number of research papers studying the physics of DWGR grating [23, 24]; however, there is still no analytical approach to work out the eigenmodes of the grating, so computer simulation is required [27].

For the (i) case, the real part of complex permittivity is now treated as zero, which means phonons cannot be excited as shown in Fig. 5(a), but there is still some loss term in the SiC material. This means that although the system has losses the resonant loss mechanism due to the excitation of SPhPs cannot operate, this scenario still allows for the excitation of DWGR albeit with slightly different dip widths due to the fact the SPhP coupling losses are eliminated. The narrow vertical dip in Fig. 5(a) and 5(b) thus clearly allows us to identify the DWGR mode in Fig. 3. If we look at Figs. 5(c) and 5(d) and compare to Fig. 3, we see that the reflectance amplitude in Fig. 5(c) gives little information as all the loss mechanisms are removed. The phase variation is almost the same as Fig. 3(b), indicating the excitation of SPhPs; following paths C and D, the difference is that the transition between different modes is slightly sharper when the loss is removed. The vertical dip at around 10.8 μm shown in Fig. 3(a) corresponds to the excitation of DWGR, where the field pattern of this resonance is similar to the field pattern of point A as shown in Fig. 8(a). The significant difference between Figs. 3 and 5 is that the vertical line in Fig. 3 is discontinuous at point B due to hybridization between DWGR and SPhPs.

We can see that the arcs corresponding to the SPhPs shown in Fig. 3 now disappear in Fig. 5(a) as expected. The FP modes are still visible at similar positions of wavelength and spacer value but with considerably greater width due to the fact that the Q of the resonator is dramatically reduced because the reflectivity between the spacer and this material (originally the SiC layer) is greatly reduced when the real part is set to zero.

3.3. Fabry-Perot (FP) resonant cavity

Since the zeroth order is a propagating order inside the spacing layer in the direction normal to the surface of the SiC, the forward propagation component will be reflected by SiC, thereby forming an asymmetrical FP cavity resonant mode. The FP resonant condition [28, 29] is given by:

$$2\beta + \phi_1 + \phi_2 = 2M\pi \tag{7}$$

where β is the phase shift upon traveling inside the cavity given by $2\pi n_s d_s/\lambda_0$, ϕ_1 is the phase angle of the reflection coefficient for incidence from the spacing layer to dielectric grating, ϕ_2 is the phase angle of the reflection coefficient at the interface between the spacing layer and the SiC, and M is standing wave mode number, M=1,2,3,...

Equation 7 allows us to work out FP cavity thickness from known ϕ_1 and ϕ_2. For this grating case, the corresponding d_s for each wavelength is shown in Fig. 6 for M=1; the thicknesses agree quite well with the arc labeled'E' in Fig. 3(a). The values of ϕ_1 and ϕ_2 were determined by calculation of the phase of reflection coefficient when the grating and the SiC were illuminated from a semi-infinite layer of spacer material.

Optics EXPRESS

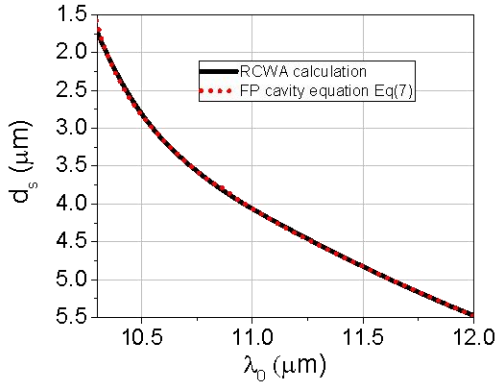

Fig. 6. shows FP cavity thickness d_s calculated using Eq. 7 (red curve) in comparison with the FP cavity position calculated using RCWA (black curve) for M=1.

3.4. Mode hybridization

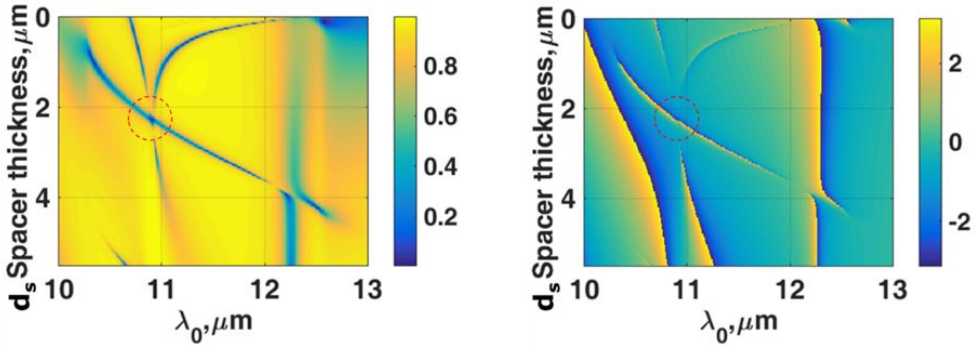

(a) (b)

Fig. 7. shows (a) zeroth order reflectance as a function of spacer made of KBr with refractive index of 1.5, thickness d_s and incident wavelength λ_0 with normal incidence and the electric field parallel to the grating vector for n_s=1.5 and (b) corresponding phase profile of the zeroth order reflectance for n_s=1.5

When two resonances occur where the k-vectors are matched, they will avoid crossing each other and form a hybridized mode [21]. Hybridized or coupled modes of the structure [30, 31] appears at the positions labeled'A and C', 'F'and 'H'in Fig. 3(a). The modes 'A and C', 'F' and 'H' are due to hybridization between SPhPs and DWGR, between DWGR and FP cavity, and between SPhPs and FP cavity, respectively. The modes labeled'A and C' is an interesting case of hybridization. Path 'A' represents a DWGR mode that is hybridized with the SPhP mode excited by the 3^{rd} order diffracted wave from the grating which beyond a separation of approximately 1.5 μm because of DWGR mode. This assertion is borne out in Fig. 5(a) where the $\Re(\varepsilon_{SiC}) = 0$. suppressing the SPhP. The DWGR curve closely follows the path 'C' in the Fig. 3(a). The path 'A' dies out soon after the hybridized point because its path is too far from other excited modes such as the SPhP. The point 'F' does not show as clear hybridization as some other cases. We confirmed its nature as hybridized mode by removing the losses of the SiC where the phase profile in the inset of Fig. 5(d) clearly shows the hybridization profile. The presence of the losses obscure this effect since the separation of the two modes is comparable to their linewidth.

Optics EXPRESS

Nevertheless, the point 'F' clearly arises from hybridization albeit in the presence of damping. The reflectance dips of these hybridized modes are normally sharper than the conventional Otto or Kretschmann configurations and this increase of sharpness does, in fact, increase the figure of merit for sensitivity when this device is used as a sensor discussed in the section 3.6.

The position of the mode hybridization can be controlled by changing the refractive index and thickness of the spacing layer and can create even a more complicated hybridized mode. For example, if the spacer was made from KBr with refractive index of 1.5 for mid-IR wavelength [26] , the SPhPs, DWGR and FP resonances occur at the same position as highlighted in dotted red circle in Fig. 7 forming hybridization between several modes.

3.5. Field distributions

For p-polarization, the two non-zero normalized E-field components, E_x and E_z, can be determined by normalized H_y, which is also parallel to the strip lines of the grating where the waveguide modes occur. We briefly discuss the characteristics of the field distributions shown in Fig. 8 that correspond to the marked points in Fig. 3.

Mode A: DWGR mode with SiC layer as energy dissipating layer, where well oriented longitudinal standing wave pattern can be observed inside the grating. The maximum $|H_y/H_{inc}|$ on the SiC surface is 6.42.

Mode B: SPhPs excited by the 4^{th} diffraction order of the grating shown in Fig. 4(b). At this operating point, it can be seen that the standing wave pattern inside the grating has been disturbed and the phonons are only weakly excited. The maximum $|H_y/H_{inc}|$ on the SiC surface is 2.60.

Mode C: SPhPs excited by the 3^{rd} diffraction order of the grating shown in Fig. 5. The field inside the grating is strongly oriented to the grating structure, but it is not so well aligned as in the pure mode A. More energy is directed towards the SiC material, which is manifested as an increase in $|H_y/H_{inc}|$ on the SiC surface. The maximum $|H_y/H_{inc}|$ on the SiC surface is 10.88.

Mode D: SPhPs excited by the 2^{nd} diffraction order of the grating. The resonance effect inside the grating has disappeared. This phononic effect is comparable to mode C with $|H_y/H_{inc}|$ on the SiC surface of 10.35.

Mode E: FP cavity standing wave pattern can be seen inside the spacing layer. $|H_y/H_{inc}|$ on the SiC surface is 1.67. This mode has its k-vector determined by the FP mode.

Mode F: Hybridized mode between DWGR and FP cavity. The maximum $|H_y/H_{inc}|$ on the SiC surface 5.17.

Mode G: FP cavity with the maximum $|H_y/H_{inc}|$ on the SiC surface is 11.95.

Mode H: Hybridized mode between SPhPs due to the 2^{nd} diffraction order of the grating and FP cavity with the maximum $|H_y/H_{inc}|$ on the SiC surface of 6.06. The FP resonant pattern was disturbed by the SPhPs and most of the energy was trapped inside the grating.

Mode I: FP cavity with the maximum $|H_y/H_{inc}|$ on the SiC surface is 11.03. The FP cavity pattern was restored after being disturbed by SPhPs as described in mode 'H'. The grating was feeding more energy to the spacing layer and dissipating energy by heat loss on the SiC layer.

Note that for the conventional Otto configuration the magnitude of $|H_y/H_{inc}|$ field distribution on the SiC surface was 1.03. Therefore the high index contrast grating coupling device can be employed to store the energy and the spacing layer can provide us a fine control to select the mode and the field strength for the SPhPs.

3.6. Sensitivity and figure of merit enhancement

The sensitivity calculation was performed by keeping the total spacing layer thickness fixed and varying the height of the coating thickness on the top of SiC layer as shown in Fig. 9.

The terms sensitivity (S) and figure of merit (FoM) are defined as: Refractive Index Sensitivity (S) is calculated as a ratio of the shift in the wavelength of a resonance with the change in sample refractive index given by: $\partial\lambda_0/\partial n_{sample}$, where λ_0 is free space wavelength where the dip

Optics EXPRESS

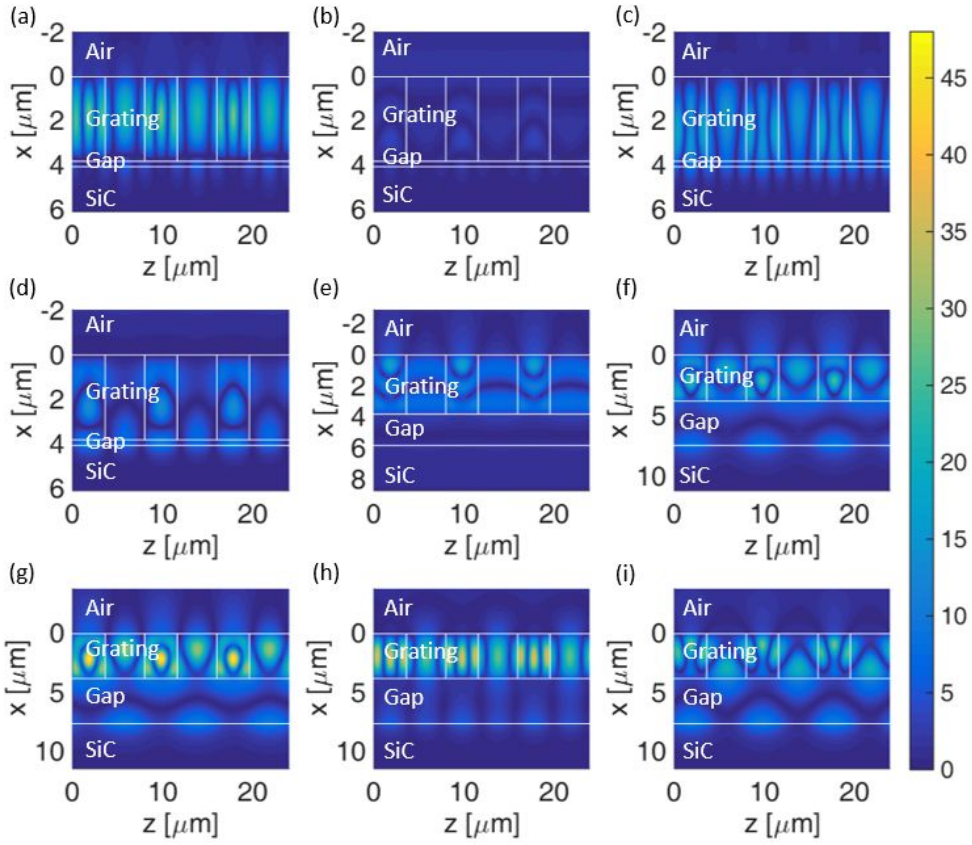

Fig. 8. shows normalized magnetic field distribution,$|H_y/H_{inc}|$, for the following operating points. (a) DWGR mode at λ_0 of 10.67 μm and d_s of 0.25 μm corresponding to 'A' in Fig. 3(a). It is clear this mode is strongly confined to the grating. (b) SPhPs excited by the 4^{th} diffracted order at λ_0 of 10.90 μm and d_s of 0.25 μm corresponding to 'B' in Fig. 3(a). (c) SPhPs excited by the 3^{rd} diffracted order at λ_0 of 11.12 μm and d_s of 0.25 μm corresponding to 'C' in Fig. 3(a). (d) SPhPs excited by the 2^{nd} diffracted order at λ_0 of 11.98 μm and d_s of 0.25 μm corresponding to 'D' in Fig. 3(a). (e) FP cavity mode at λ_0 of 10.34 μm and d_s of 2.00 μm corresponding to 'E' in Fig. 3(a). (f) Hybridized position between DWGR and FP cavity at λ_0 of 10.79 μm and d_s of 3.66 μm corresponding to 'F' in Fig. 3(a). (g) FP cavity at λ_0 of 10.85 μm and d_s of 3.82 μm corresponding to 'G' in Fig. 3(a). (h) Hybridized position between SPhPs excited by the 2^{nd} diffracted order and FP cavity at λ_0 of 10.87 μm and d_s of 3.82 μm corresponding to 'H' in Fig. 3(a). (i) FP cavity at λ_0 of 10.90 μm and d_s of 3.82 μm corresponding to 'I' in Fig. 3(a).

occurs and n_{sample} is the refractive index of the sample layer refractive index. FoM accounts for the sharpness of the reflectance dip and the magnitude of sensitivity, and is defined as $S/FWHM$, where S is the refractive index sensitivity and FWHM is the full width at half maximum of the reflectance dip.

In this section, we compare the sensitivity and figure of merit of the modified grating coupled Otto configuration with conventional Otto configuration for 0.25 μm spacer thickness to demonstrate the device sensitivity and figure of merit enhancement. There are 3 modes for this thickness as show in Fig. 3(a) DWGR mode at 10.67 μm (labeled 'A' in Fig. 3(a)), SPhPs excited by the 3^{rd} diffracted order at 11.12 μm (labeled 'C' in Fig. 3(a)) and SPhPs excited by the 2^{nd}

Optics EXPRESS

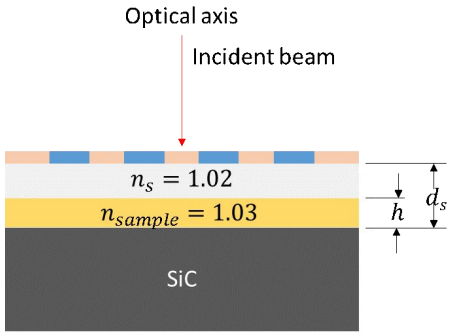

Fig. 9. shows local refractive index sensitivity measurement method.

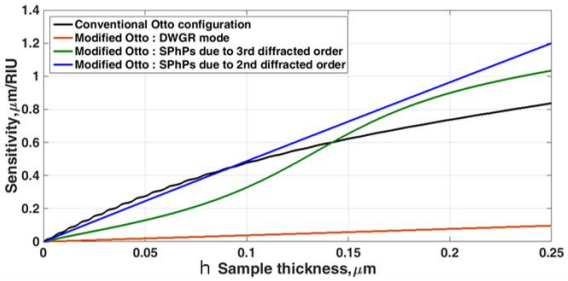

(a)

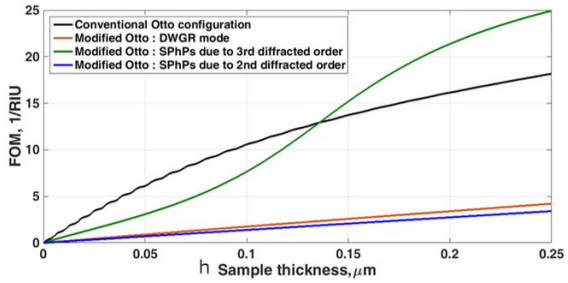

(b)

Fig. 10. shows (a) sensitivity and (b) figure of merit for a hybrid device with spacing layer made of LiF of 0.25 μm thickness. The local refractive index on the top of SiC material was varied by changing the refractive index of LiF from 1.02 to 1.03 [32] with varied thickness h.

diffracted order at 11.98 μm (labeled 'D' in Fig. 3(a)) respectively.

Figure 10(a) shows that the DWGR mode is not sensitive to local refractive index change, whereas the other two modes can provide comparable sensitivity to the conventional Otto system. The sensitivity for the modified SPhPs is better than the conventional Otto for the coating thickness greater than 90 nm for the SPhPs excited by the 2^{nd} diffracted order and 140 nm for the 3^{rd} diffracted order respectively. However, the dip of the SPhPs excited by the 2^{nd} evanescent order is not as deep as the conventional Otto and the SPhPs mode due to the 3^{rd} evanescent order; hence the FOM performance of the 2^{nd} evanescent order is worse than the conventional mode. The FOM performance of the SPhPs excited by the 3^{rd} evanescent order is significantly

Optics EXPRESS

better than the conventional Otto, giving rise to sensitivity enhancement of 43.32% and FOM enhancement of 37.18% respectively. The reasons that this structure can provide sensitivity and FOM enhancement are that (i) the SPhPs field is confined within the spacing layer gap as shown in Fig. 8(c) and (d) and (ii) the reflectance dip excited by this structure is sharper (smaller FWHM) than the conventional one due to guided mode resonance.

The sensor structure described here has several potential sensor applications. One example is for gas sensing, which could be implemented using a porous spacer layer where the analyte diffuses in changing the average refractive index. Another application is for ultrasonic and pressure sensing where the change in the gap separation is detected by the change in reflectivity. Operating close to one of the positions of mode hybridization with SPhPs will give enhanced sensitivity. Further investigations of parameter space maybe expected to give further sensitivity enhancements, especially as the method provides considerable flexibility in the choice of parameters.

4. Conclusion

We have numerically demonstrated that a modified grating-coupled Otto configuration system enables us to excite different resonance modes and hybridized modes with no requirement of plasma etching the phononic material. Since the excitation was applied through a series of k-vectors due to grating diffracted orders, this allows us to excite more than one SPhP mode simultaneously. Controllable operating position of resonances can be realized by changing the refractive index and thickness of the spacing layer. It can also enhance the field strength of SPhPs on the surface of a phononic material by a factor 10 compared to the conventional Otto mode; this is due to the energy trapped inside the high index contrast grating. Although the structure studied here is a solid spacing layer as we are interested in developing an ultrasonic/pressure sensor, the method is applicable to fluid sensing by either reverting to Kretschmann configuration, albeit with the problems of material quality referred to in the introduction or using a porous spacer layer. We finally demonstrate that the field confinement within the spacing gap can enhance the sensitivity and figure of merit performance for local refractive index sensing application. It is important to note that this idea is not limited to SPhPs, but also applicable to other types of surface waves, such as, SPPs.

Funding

We wish to acknowledge funding from the following sources: The Hong Kong Polytechnic University (1-ZE23); Hong Kong GRF Project (15210515), ‘Grating Technologies for Advanced Optical microscopy’.